Design and optimization of a novel organic Rankine cycle with improved boiling process

Andreasen, Jesper Graa; Larsen, U.; Knudsen, Thomas; Haglind, Fredrik

Published in:
Energy

Link to article, DOI:
10.1016/j.energy.2015.06.122

Publication date:
2015

Document Version
Peer reviewed version

Design and optimization of a novel organic Rankine cycle with improved boiling process

J.G. Andreasen[a,*], U. Larsen[b], T. Knudsen[a], F. Haglind[a]

[a] *Technical University of Denmark, Department of Mechanical Engineering Building 403, Nils Koppels Allé, DK-2800 Kgs. Lyngby, Denmark*

[b] *Chalmers University of Technology, Maritime Operations, SE-412 96 Gothenburg, Sweden*

Abstract

In this paper we present a novel organic Rankine cycle layout, named the organic split-cycle, designed for utilization of low grade heat. The cycle is developed by implementing a simplified version of the split evaporation concept from the Kalina split-cycle in the organic Rankine cycle in order to improve the boiling process. Optimizations are carried out for eight hydrocarbon mixtures for hot fluid inlet temperatures at 120 °C and 90 °C, using a genetic algorithm to determine the cycle conditions for which the net power output is maximized. The most promising mixture is an isobutane/pentane mixture which, for the 90 °C hot fluid inlet temperature case, achieves a 14.5 % higher net power output than an optimized organic Rankine cycle using the same mixture. Two parameter studies suggest that optimum conditions for the organic split-cycle are when the temperature profile allows the minimum pinch point temperature difference to be reached at two locations in the boiler. Compared to the transcritical organic Rankine cycle, the organic split-cycle improves the boiling process without an entailing increase in the boiler pressure, thus enabling an efficient low grade heat to power conversion at low boiler pressures.

Keywords: organic split-cycle, genetic algorithm, novel power cycle, zeotropic mixtures, low grade heat

1. Introduction

Compared to the steam Rankine cycle, the organic Rankine cycle (ORC) is a more appropriate technology for conversion of low grade heat into electric power [1], but, due to

*Corresponding author. Tel.: +45 45 25 41 23

Email address: jgan@mek.dtu.dk (J.G. Andreasen)

Nomenclature

Acronyms

ARC	Auto-cascade Rankine cycle
Bp	Bubble point
ORC	Organic Rankine cycle
OSC	Organic split-cycle

Greek symbols

Δ	Difference
η	Efficiency

Symbols

A	Area, [m^2]
h	Mass specific enthalpy, [kJ/kg]
$\dot{m}$	Mass flow rate, [kg/s]
n	Number of discretization points, [-]
P	Pressure, [bar]
$\dot{Q}$	Heat transfer rate, [kW]
T	Temperature, [°C]
$\bar{U}$	Average overall heat transfer coefficient, [kJ/kgK]
$\dot{W}$	Power, [kW]
x	Vapour quality, [-]
X	Mole composition, [-]
Y	Mass composition, [-]

Subscripts

boil	Boiler
cond	Condenser
cool	Cooling water
eff	Effective
evap	Evaporator
exp	Expander
g	Glide
hf	Hot fluid
i	Inlet
intm	Intermediate
l	Lean
min	Minimum
NET	Net
o	Outlet
p	Polytropic
pump	Pump
r	Rich
recu	Recuperator
s	Isentropic
tot	Total
wf	Working fluid

thermodynamic limitations, it is challenging to achieve high heat to power conversion efficiencies when the heat source inlet temperature is low. A crucial aspect of maximizing system efficiency is to reduce heat transfer irreversibilities, which correlate with the temperature difference between the heat exchanging streams. The irreversibilities are minimized when the temperature profiles of the streams are optimally matched. Pure fluids are traditionally used as working fluids in ORCs; however, the isothermal evaporation and condensation at subcritical pressures do not enable an optimal temperature profile match in the condenser or the boiler, when the heat source and heat sink are non-isothermal. In the scientific literature different methods for reducing heat transfer irreversibilities of condensation and boiling have been suggested. In transcritical cycles the temperature profile is improved by adopting a supercritical boiler pressure, thereby eliminating the isothermal two-phase evaporation at the expense of relatively high cycle pressures [2, 3]. By implementing a zeotropic mixture as the working fluid, it is possible to evaporate and condense the working fluid non-isothermally at subcritical pressures. This enables a reduction in the temperature difference between the heat exchanging streams both for the condenser and the boiler resulting in an increase in cycle performance [4]. Analyses of the irreversibilities in the cycle components have identified the condenser as achieving the largest benefits from the non-isothermal phase-change, and the mixture composition minimizing the condenser losses tends to coincide with the

composition which maximizes cycle performance [5, 6]. In a recent study, Weith et al. [7] investigated the potential of using a siloxane mixture (MM/MDM) as the working fluid for an ORC utilizing the 460 °C exhaust heat from a biogas engine. By using the mixture they obtained an increase in the second law efficiency of 3 % for combined heat and power generation and 1.3 % for electricity generation compared to pure MM. Chys et al. [8] showed that the relative increase in cycle efficiency for mixtures compared to pure fluids decreases when the heat source inlet temperature increases. For a 150 °C inlet temperature they reported a cycle efficiency increase of 15.7 % when using binary mixtures instead of pure fluids.

Using a zeotropic mixture, it is possible to modify the properties of the working fluid by changing the composition of the mixture within the cycle. In the Kalina cycle a separator is implemented to separate the vapour and liquid phases of a two-phase ammonia/water stream, enabling the creation of two streams with different compositions. The review by Zhang et al. [9] provides an overview of the literature on Kalina cycle systems in which many different cycle layouts have been proposed and analysed. Hettiarachchi et al. [10] investigated a simple Kalina cycle with a separator placed between the evaporator and the expander for utilization of a low temperature heat source at 90 °C. Compared to two ORCs with ammonia and isobutane as the working fluids, the overall performance of the Kalina cycle was found to be higher. Bombarda et al. [11] compared the performance of a Kalina cycle, with the separator located at an intermediate pressure level, and an ORC for utilization of diesel engine waste heat at 346 °C. They found that the two cycles produced similar power outputs, while the pressure in the Kalina cycle was significantly higher than in the ORC. Modi and Haglind [12, 13] optimized four Kalina cycles for utilization of concentrated solar energy (expander inlet temperature over 450 °C). They found that the cycle layout with the most recuperators obtained the highest cycle efficiency. Bao and Zhao [14] developed a novel cycle layout based on the Kalina cycle: the auto-cascade Rankine cycle (ARC). In this cycle a separator generates a vapour stream, which is superheated and expanded, and a liquid stream, which is evaporated in an internal heat exchanger and subsequently expanded in a second expander. For a geothermal heat source the ARC obtained an exergetic efficiency of 59.12 %, while an ORC obtained 52 % and a Kalina cycle 44 %.

In addition to the Kalina cycle, Alexander Kalina developed the split-cycle concept [15] by also implementing a separator to generate a saturated vapour stream and a saturated liquid stream at different compositions. The vapour and liquid streams are split and mixed until two working fluid streams with desired compositions are created. The two working fluid streams are then evaporated simultaneously in a multi-stream evaporator, such that

the pinch point (normally at the saturated liquid point) is smoothened. This makes it possible either to increase the boiler pressure or increase the working fluid mass flow and thereby increase the power output of the cycle. Larsen et. al. [16] modelled the Kalina split-cycle and found that the Kalina split-cycle with reheat obtained an increase in power output of 11.4 % compared to a reference Kalina cycle without reheat. Nguyen et al. [17] used an exergy analysis to compare the Kalina split-cycle and the Kalina cycle, and found that the irreversibilities in the Kalina split-cycle were 2.5-5 % lower than the irreversibilities in the Kalina cycle, primarily due to an improvement of the boiling process.

In this paper we present a novel organic Rankine cycle layout, named the organic split-cycle (OSC), which is based on a simplification of the Kalina split-cycle. The OSC also includes the multi-stream evaporator, but implements a simplified method for the split stream generation. The paper encompasses an optimization study, two parameter studies, initial considerations on the design of the multi-stream evaporator and a comparison of the OSC process to the ORC and the Kalina split-cycle processes. In the optimization study, eight hydrocarbon mixtures are optimized to maximize the net power output from utilization of a 120 °C and a 90 °C water stream representing either waste heat or geothermal water streams. In the parameter studies, we investigate how selected design parameters affect the location of the pinch points in the boiler, and ultimately how these affect the performance of the cycle. The analysis of the multi-stream evaporator illustrates the necessary $\bar{U}A$ distribution in order to achieve the desired temperature profile, and provides the basis for a discussion on the design requirements for this heat exchanger.

The paper begins with a description of the OSC process in Section 2. The modelling methodology is outlined in Section 3, and in Section 4 the results from the analyses are presented and discussed. Conclusions are given in Section 5.

2. Organic split-cycle

The OSC process results from an implementation of the thermodynamically beneficial split-stream evaporation in an ORC process; see Fig. 1 (a). The split streams are generated and directed to the boiler section (preheater, superheater, evaporators 1 and 2) in a simple manner, in order to limit the complexity of the system. From state 4 to state 3 (through 5, 6, 7, 1 and 2), the OSC contains the same components as the traditional recuperated ORC. The recuperator partially evaporates the working fluid and delivers the working fluid in a two-phase state to the separator (state 3). In the separator, the liquid and vapour phases are separated in a liquid stream (state 8) with a low concentration of the more volatile

component (the lean stream) and a vapour stream (state 11) with a high concentration of the more volatile component (the rich stream). The lean stream is pressurized to the boiler pressure (state 9), and the rich stream is first condensed (state 12), pressurized to the boiler pressure (state 13) and then preheated (state 14) to the same temperature as the pressurized lean stream in state 9, i.e., $T_{14} = T_9$. At the outlet of evaporator 1 the two streams are mixed (state 4), and the boiling process is completed in evaporator 2 and the superheater (superheating is optional) until the specified expander inlet state is reached in state 5.

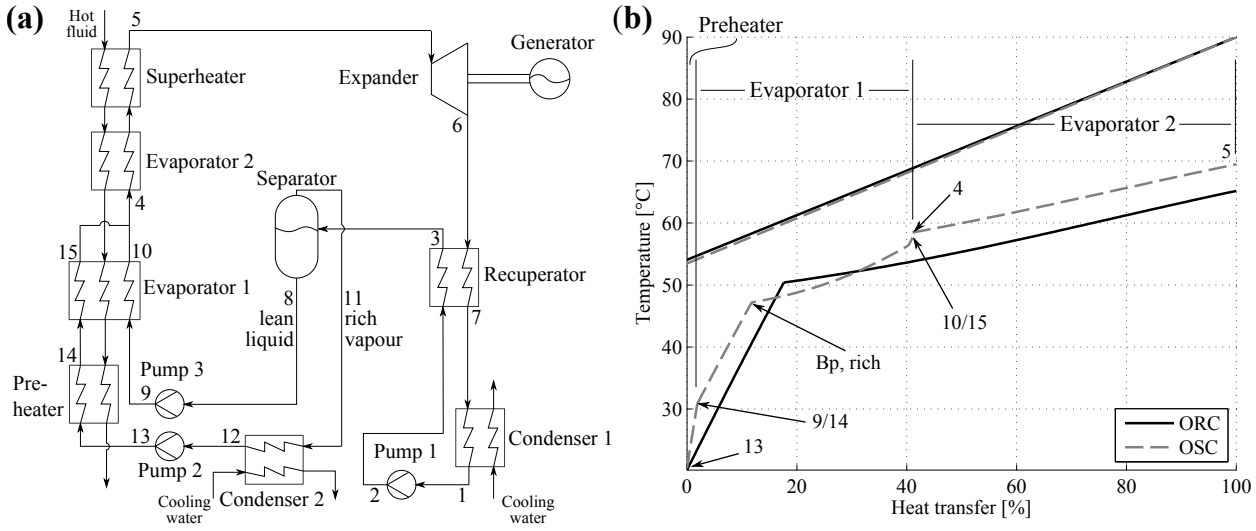

Figure 1: (a) a sketch of the OSC and (b) a comparison of the boiling process of the ORC and the OSC illustrated in a $\dot{Q}T$-diagram with indications of the preheater, evaporator 1 and 2 included for the OSC

Figure 1 (b) shows a $\dot{Q}T$-diagram for the boiling process in an ORC and an OSC, both using the same working fluid with the same outlet composition, and both delivering the working fluid in a saturated vapour state, $x_5 = 1$. The saturated vapour condition at the boiler outlet (state 5) does not necessarily represent the optimal solution for the OSC, but it is implemented here in order to simplify the $\dot{Q}T$-diagram and clarify the differences between the boiling processes of the ORC and the OSC. In the OSC, superheating can be used to increase the enthalpy at the expander outlet and thereby increase the available amount of heat for the recuperator. This can be necessary for wet fluids, but whether superheating is beneficial or not should be determined based on cycle optimizations. In Fig. 1 (b) the working fluid in the ORC is first preheated and then evaporated, where the transition from preheating to evaporation is recognised as the sudden slope change. When the temperature profile of the hot fluid is linear, this point is typically also the location of the minimum pinch point temperature difference representing a limitation for the heat transfer process.

In the last part of the boiling process (from state 4 to 5), the working fluid compositions of the ORC and the OSC are the same, and the higher temperature of the OSC therefore represents a boiler pressure difference between the ORC and the OSC. Even though the boiler pressure is higher in the OSC, the higher concentration of the more volatile component in the rich stream makes it possible to start evaporation at a lower temperature, thus enabling a pressure increase without violating the minimum pinch point temperature difference of the boiler. Compared to the ORC, the temperatures are higher for the OSC through most of the boiling process, while the hot fluid temperature profiles for the two cycles are similar. This enables an overall reduction in the temperature difference between the heat exchanging streams, thereby reducing irreversibilities in the OSC boiler.

How to divide optimally the heating load between evaporators 1 and 2, is not immediately predictable. For the Kalina split-cycle, Kalina [15] argued that it is thermodynamically beneficial to define the rich and lean streams at the outlets of evaporator 1 to be at the dew point and the bubble point, respectively. In the Kalina split-cycle it is possible to set the conditions at both outlets, since the additional components make it possible to dictate the composition of the rich and the lean stream. In the OSC the compositions of the rich and the lean stream are given directly from the condition at the separator inlet, and it is therefore only possible to select the condition at one of the outlets from evaporator 1.

3. Methodology

The working principle of the OSC is based on a modification to the temperature profile of subcritical boiling and it is therefore necessary that the working fluid pressure is subcritical. It is desirable that the working fluid is dry, since this enables more heat to be recuperated from the expander exhaust. Binary mixtures containing propane, butane, isobutane, pentane or isopentane provide these properties (propane is not dry but when mixed with either of the four other fluids dry mixtures can be formed) and have demonstrated high performance in ORC applications [18]. Mixtures of these fluids are therefore selected as working fluids in the present study.

The thermodynamic models were developed in Matlab® 2012b [19] using the commercial software REFPROP® version 9.0 [20] for thermodynamic property data. REFPROP® includes implementations of the equations of state which are necessary to obtain property data for the selected working fluids [21–25]. The optimizations were carried out using a genetic algorithm optimizer, with the same settings as those used in ref. [18].

For all optimizations the genetic algorithm is run through 200 generations, with the net

power output as the objective function. The net power is calculated as

$$\dot{W}_{NET} = \dot{m}_{wf}[h_5 - h_6 - (h_2 - h_1)] - \dot{m}_l(h_9 - h_8) - \dot{m}_r(h_{13} - h_{12}) \quad (1)$$

where $\dot{m}$ is mass flow, h is mass specific enthalpy, subscript wf denotes the working fluid through the expander, r denotes rich stream and l denotes lean stream.

Table 1: Optimization parameters

Parameter description	Symbol	Range
Expander inlet temperature	T_5	20 °C ÷ 110/80 °C
Expander inlet pressure	P_5	1 bar ÷ 15/30 bar
Mole composition	X_{wf}	0 ÷ 1
Intermediate pressure	P_{intm}	P_1 ÷ P_5
Evaporator 1 outlet temperature	T_{10}	20 °C ÷ 110/80 °C

The parameters subject to optimization are the following: the expander inlet temperature (T_5), the expander inlet pressure (P_5), the composition of the mixture (X_{wf}), the intermediate pressure (P_{intm}) and the outlet temperature of evaporator 1 (T_{10}); see Table 1. The upper limit on the expander inlet temperature and the temperature at the outlet of evaporator 1 are dependent on the hot fluid inlet temperature, and the upper limit for the expander inlet pressure (boiler pressure) is 30 bar for mixtures including propane and 15 bar for other mixtures. The pressure ranges are selected such that the optimum expander inlet pressures are not located near the boundaries. As a reference to the OSC optimizations, optimizations of recuperated ORCs are carried out for each of the considered mixtures. The relative increase in net power of the OSC compared to the ORC is calculated as

$$\Delta\dot{W}_{NET} = \frac{\dot{W}_{NET,OSC} - \dot{W}_{NET,ORC}}{\dot{W}_{NET,ORC}} \quad (2)$$

The heat transfer area needed is compared for the ORC and the OSC processes based on $\bar{U}A$-values, which is the product of the overall average heat transfer coefficient ($\bar{U}$) and the heat transfer area (A). In order to compare directly the heat transfer areas, heat exchanger designs would need to be carried out for the heat exchangers such that $\bar{U}$ could be evaluated, but this is outside the scope of the present study. Since the $\bar{U}A$-values are only compared for ORCs and OSCs using the same working fluids, it is reasonable to expect the $\bar{U}$-values for the two cycles to be similar. The relative difference in $\bar{U}A$-values is calculated as

$$\Delta\bar{U}A = \frac{\bar{U}A_{OSC} - \bar{U}A_{ORC}}{\bar{U}A_{ORC}} \quad (3)$$

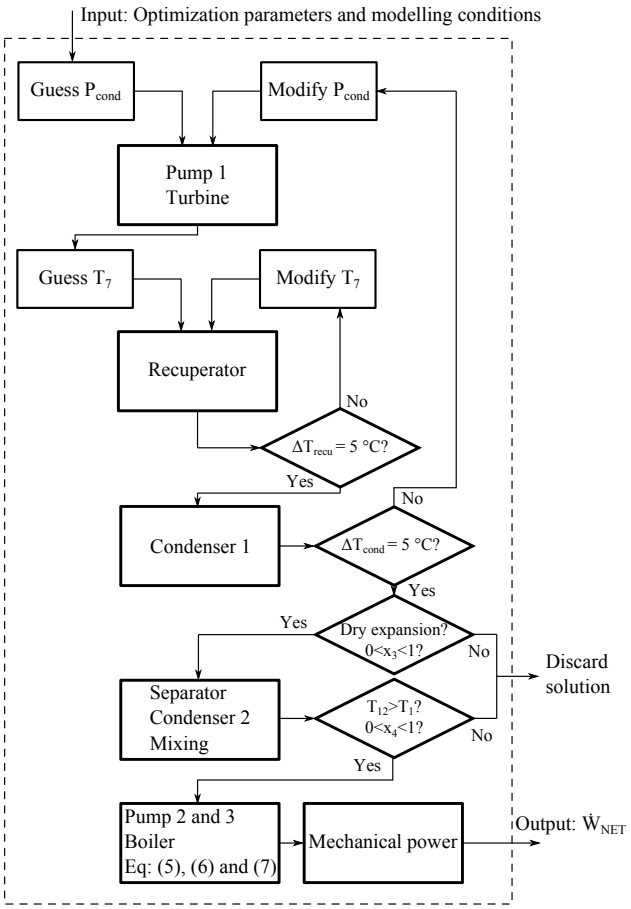

Figure 2: Flow chart illustrating the model structure

In the ORC optimizations the net power is maximized by optimizing the expander inlet temperature and pressure and the mixture composition. The modelling conditions for the reference ORC are the same as for the OSC (see also ref. [18]).

An overview of the numerical model is illustrated in Fig. 2, and the modelling conditions are listed in Table 2. The OSC is modelled assuming fixed pinch points for the heat exchangers, isentropic efficiencies for the pumps and a polytropic efficiency for the expander. Additional assumptions are the following: no pressure loss in piping or heat exchangers, no heat loss from the system, steady state condition and homogeneous flow in terms of thermodynamic properties.

The first part of the model consists of two iterative procedures to determine the condensation pressure and the hot fluid outlet temperature of the recuperator (T_7), such that the specified minimum pinch point temperatures in both heat exchangers are satisfied; see Fig. 2. When convergence is reached, it is checked that the expansion does not enter the

Table 2: Modelling conditions

Parameter description	Symbol	Value
Hot fluid (water)		
Hot fluid inlet temperature	$T_{hf,i}$	120 °C & 90 °C
Hot fluid mass flow	$\dot{m}_{hf}$	50 kg/s
Hot fluid pressure	P_{hf}	4 bar
Condenser 1		
Cooling water inlet temperature	$T_{cool,i}$	15 °C
Cooling water temperature rise	ΔT_{cool}	5 °C
Min. temperature difference	ΔT_{cond}	5 °C
Outlet vapour quality	x_1	0
Cooling water pressure	P_{cool}	4 bar
Control volumes in discretization	n_{cond}	10
Pumps		
Isentropic efficiency	$\eta_{s,pump}$	0.8
Recuperator		
Min. temperature difference	ΔT_{recu}	5 °C
Separator		
Outlet vapour quality, liquid	x_8	0
Outlet vapour quality, vapour	x_{11}	1
Condenser 2		
Outlet vapour quality	x_{12}	0
Boiler		
Min. temperature difference	ΔT_{boil}	10 °C
Expander		
Polytropic efficiency	$\eta_{p,exp}$	0.8
Min. vapour quality	$x_{exp,min}$	1
Control volumes in discretization	n_{exp}	50

two-phase region and that a two-phase state is obtained at state 3. From a given inlet to the separator, the thermodynamic outlet conditions, along with the compositions of the rich and lean streams, are determined. From the condition $x_{12} = 0$ and the intermediate pressure, the outlet temperature of condenser 2 is determined, and h_4 is determined from the energy balance of mixing

$$h_4 = h_{10}\frac{Y_{wf} - Y_r}{Y_l - Y_r} + h_{15}\left(1 - \frac{Y_{wf} - Y_r}{Y_l - Y_r}\right) \tag{4}$$

where Y is the mass fraction of the more volatile component, the enthalpies are determined knowing the boiler pressure, and $T_{10} = T_{15}$ and the mass flows have been eliminated using the mass balances

$$\dot{m}_{wf} = \dot{m}_r + \dot{m}_l \tag{5}$$

$$Y_{wf}\,\dot{m}_{wf} = Y_r\,\dot{m}_r + Y_l\,\dot{m}_l \tag{6}$$

In order to ensure that the inlet to evaporator 2 is in a two-phase state and that the temperature at the outlet of condenser 2 is not too low for the available heat sink, it is checked that $0 < x_4 < 1$ and $T_{12} > T_1$. If these conditions are met, the isentropic pump efficiency is used to determine the outlet states of pumps 2 and 3. All inlet and outlet states to the boiler on the working fluid side are thereby determined, and the specified pinch point for the boiler is used to obtain the hot fluid outlet temperature. The mass flows in the system are then determined from the energy balance over the boiler and the mass balances in equations (5) and (6)

$$\dot{m}_{wf} = \frac{\dot{m}_{hf}(h_{hf,i} - h_{hf,o})}{h_5 - h_{13}\left(1 - \frac{Y_{wf}-Y_r}{Y_l-Y_r}\right) - h_9\frac{Y_{wf}-Y_r}{Y_l-Y_r}} \tag{7}$$

$$\dot{m}_r = \dot{m}_{wf}\left(1 - \frac{Y_{wf} - Y_r}{Y_l - Y_r}\right) \tag{8}$$

$$\dot{m}_l = \dot{m}_{wf}\frac{Y_{wf} - Y_r}{Y_l - Y_r} \tag{9}$$

where subscript hf denotes hot fluid.

In order to increase the computational speed, the discretizations of the boiler and the recuperator are only carried out for selected points, where the pinch points are likely to occur. For the recuperator, the inlet and outlet points are included in the discretization along with the possible dew point for the hot stream and the bubble point for the cold steam. For the boiler, the selected points are the following: the inlet and outlet states (state 13 and state 5), the bubble point in the preheater (when $x_{14} > 0$), the inlet and outlet of evaporator 1 (states 14/9 and states 15/10), the inlet to evaporator 2 (state 4), the bubble point for the rich stream (when $x_{15} > 0$) and the bubble point for the lean stream (when $x_{10} > 0$). Checking the pinch points at these locations is adequate if the curvatures of the temperature profiles are limited. The sufficiency of this approach is verified for each optimized solution, by comparing the results to simulations where the temperature difference is checked at 100 locations (with equal enthalpy spacings between the cold side inlet and outlet) for the boiler and the recuperator.

Figure 3 shows the points which are selected for the boiler discretization in two $\dot{Q}T$-diagrams. The $\dot{Q}T$-diagram in Fig. 3 (a) displays a case where the evaporation begins in evaporator 1. In this case the pinch point is checked in the following locations: state 13, state 9 and 14, the rich stream bubble point (Bp, rich), the lean stream bubble point (Bp,

lean), state 10 and 15, state 4 and state 5. In the $\dot{Q}T$-diagram displayed in Fig. 3 (b) the preheater make up a larger part of the total heat transfer, and in this case the evaporation starts in the preheater. Here, the pinch point is checked in the following locations: state 13, bubble point in the preheater (Bp, preheater), state 9 and 14, state 10 and 15, state 4 and state 5.

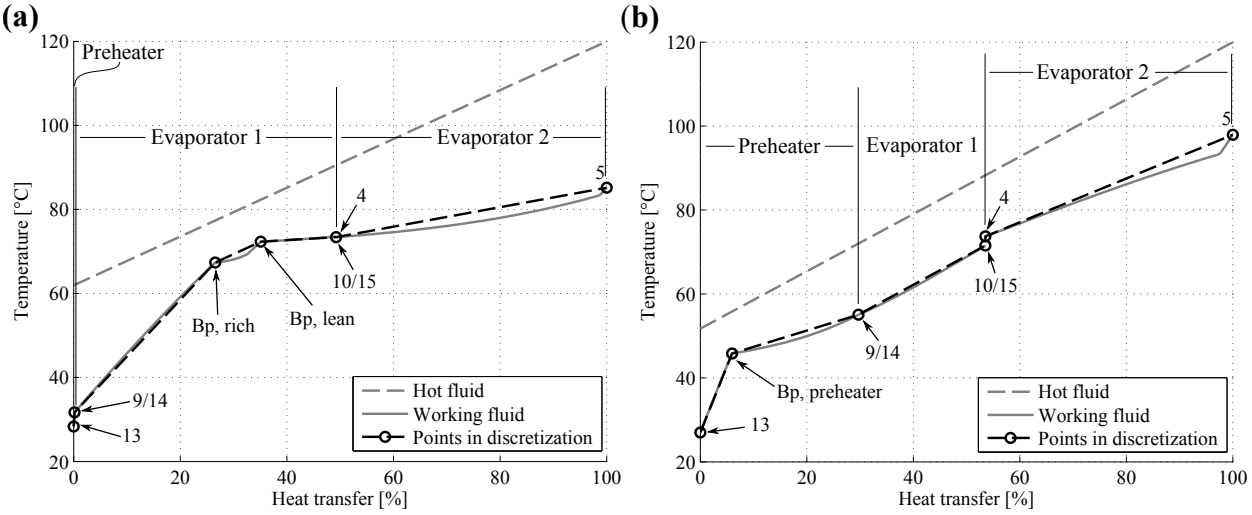

Figure 3: $\dot{Q}T$-diagrams of the OSC boiler for two cases displaying the points included in the discretizations

4. Results and discussion

Tables 3 and 4 list the results from the optimization of eight different hydrocarbon mixtures when the hot fluid inlet temperature is 120 °C and 90 °C. For the case where $T_{hf,i}$ = 120 °C the maximum net power output is obtained by the propane/isobutane mixture. The mixture isobutane/pentane reaches the highest relative increase at 6.4 % for the OSC compared to an optimized ORC using the same mixture.

The OSC optimizations carried out for the $T_{hf,i}$ = 90 °C case indicate that the split evaporation concept is more beneficial when the hot fluid inlet temperature is low. The thermodynamically best performing fluid is the isobutane/pentane mixture with $\dot{W}_{NET}$ = 567 kW and a relative net power increase of 14.5 % compared to the corresponding ORC. For propane/isopentane and propane/pentane, the OSCs also reach net power outputs which are more than 10 % larger than the net power outputs of the ORCs.

In an ORC the condenser is usually the component that benefits the most from using zeotropic mixtures, and the mixture composition which maximizes cycle performance tends to coincide with the composition which results in optimal conditions for the condenser.

Optimal performance for the condenser is reached when the temperature difference is at a minimum, i.e. when the temperature glide of condensation matches the temperature increase of the cooling water [5]. For the OSC the temperature glide of condensation (ΔT_g) is only close to the temperature increase of the cooling water for butane/isopentane and propane/isobutane. For the remaining mixtures, the temperature glide is significantly larger than the cooling water temperature increase, resulting in non-optimal conditions for the condenser. This suggests that the influence of the condensation process, in determining the optimum composition, is less pronounced for the OSC compared to the ORC.

Table 3: Optimization results for different working fluid mixtures for a 120 °C hot fluid inlet temperature

Fluids	P_5 [bar]	T_5 [°C]	X_{wf} [-]	P_2 [bar]	T_{10} [°C]	ΔT_g [°C]	$\dot{m}_{wf}$ [kg/s]	$\dot{m}_r$ [kg/s]	$\dot{W}_{NET}$ [kW]	$\Delta\dot{W}_{NET}$ [%]
ibut/ipen	9.0	79.2	0.73	2.8	72.5	9.9	30.3	3.1	1232	6.0
but/ipen	6.1	79.5	0.61	1.8	69.4	6.3	28.3	2.4	1223	5.9
ibut/pen	6.6	84.3	0.49	2.4	72.6	17.7	30.6	7.0	1233	6.4
but/pen	5.4	91.3	0.58	1.8	68.7	10.4	27.2	3.8	1206	5.0
pro/ibut	21.0	89.2	0.69	7.4	71.5	6.6	30.3	2.7	1249	3.3
pro/but	22.2	86.5	0.83	7.9	70.2	8.5	30.8	2.3	1241	3.0
pro/ipen	23.5	86.7	0.86	9.5	77.8	19.3	31.1	3.4	1226	2.3
pro/pen	24.4	83.1	0.92	9.7	79.7	17.3	31.8	2.1	1223	2.4

Table 4: Optimization results for different working fluid mixtures for a 90 °C hot fluid inlet temperature

Fluids	P_5 [bar]	T_5 [°C]	X_{wf} [-]	P_2 [bar]	T_{10} [°C]	ΔT_g [°C]	$\dot{m}_{wf}$ [kg/s]	$\dot{m}_r$ [kg/s]	$\dot{W}_{NET}$ [kW]	$\Delta\dot{W}_{NET}$ [%]
ibut/ipen	5.1	78.1	0.65	2.6	51.5	11.3	20.1	4.1	545	9.3
but/ipen	3.8	77.1	0.62	1.8	50.5	6.2	18.4	2.5	538	7.5
ibut/pen	5.2	68.1	0.62	2.6	57.0	16.6	20.1	6.1	567	14.5
but/pen	4.2	79.6	0.75	1.9	51.7	8.4	17.4	2.5	537	8.6
pro/ibut	14.1	79.9	0.72	7.4	51.3	6.3	19.3	2.6	546	8.3
pro/but	14.7	79.6	0.79	7.8	52.2	9.7	18.9	3.1	549	9.8
pro/ipen	15.3	74.6	0.81	8.7	57.3	24.0	19.7	5.4	553	11.8
pro/pen	15.7	75.8	0.85	9.4	63.2	26.4	19.2	4.8	545	10.7

In general, the mass flow rate of the rich stream is small compared to the mass flow rate of the lean stream. A high rich stream mass flow means that a large amount of heat must be exchanged in condenser 2 resulting in large exergy losses. The mass flow of the rich stream must therefore be low, such that the exergy losses in condenser 2 does not cancel out the benefits of the split stream evaporation.

4.1. Parameter studies

The optimizations presented in Tables 3 and 4 indicate the potential of the OSC; however, no information regarding the influence of the optimized parameters on the cycle is

obtained from these results. In the succeeding subsections, parameter studies, focussed on the influence of the intermediate pressure (P_2) and the temperature after evaporator 1 (T_{10} and T_{15}), are presented. The analysis is based on the low temperature $T_{hf,i} = 90$ °C case, for the OSC using the mixture isobutane/pentane (0.62/0.38) as a working fluid, since the optimizations identified this fluid and hot fluid inlet temperature as the most promising.

4.1.1. Intermediate pressure

Figure 4 (a) depicts the variation of the net power output as a function of the boiler pressure (P_5) and the intermediate pressure (P_2), for the isobutane/pentane (0.62/0.38) mixture with $x_{10} = 0$ and $x_5 = 1$. The condition at state 10 is fixed as saturated liquid, and state 5 is saturated vapour in order to limit the degrees of freedom in the analysis. For each of the plotted solutions a square indicates a boiler pinch point location at the bubble point for the rich stream, and an asterisk indicates a boiler pinch point location at the outlet of evaporator 1.

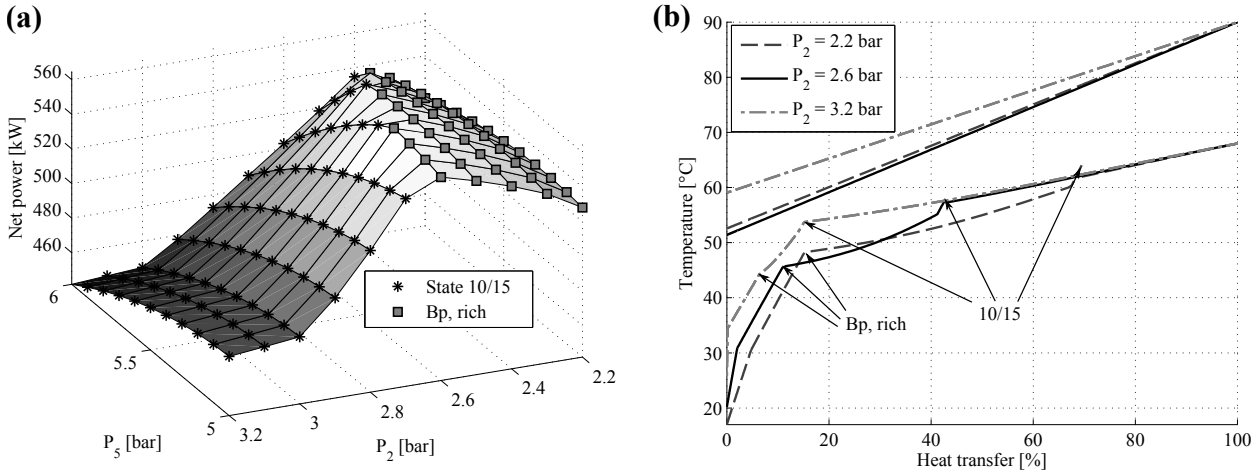

Figure 4: (a) a plot of the net power as a function of P_5 and P_2 for the OSC with an isobutane/pentane (0.62/0.38) mixture as the working fluid and (b) a $\dot{Q}T$-diagram of the boiler for three intermediate pressures with $P_5 = 5.3$ bar

For the case where $P_2 = 2.2$ bar, the intermediate pressure is just larger than the condensation pressure, $P_1 = 2.1$ bar. In this case, the boiler pinch point is located at the bubble point for the rich stream, i.e. in evaporator 1. By increasing the intermediate pressure, the vapour quality at the recuperator outlet (state 3) is reduced, giving a lower amount of separated rich vapour with a higher concentration of the more volatile component. This results in a reduction in the bubble point temperature of the rich stream and a reduction in the heat requirement to reach the bubble point for the rich stream. Additionally, with

the condition $x_{10} = 0$ fixed, an increase in the intermediate pressure results in a higher concentration of the lean stream entailing a lower bubble point temperature and a lower heat requirement in order to reach the specified condition at state 10.

The impact of these relationships is illustrated in Fig. 4 (b), where $\dot{Q}T$-diagrams for the boiler at intermediate pressures of $P_2 = 2.2$ bar, $P_2 = 2.6$ bar and $P_2 = 3.2$ bar, all for a boiler pressure at $P_5 = 5.3$ bar, are shown. Since it requires less heat to reach the bubble points for the rich and lean streams and the bubble point temperatures decrease when the intermediate pressure increases, the location of the bubble points moves in a direction toward the lower left in the $\dot{Q}T$-diagram as the intermediate pressure increases. For the case where $P_2 = 2.2$ bar, the pinch point is located at the bubble point for the rich stream, and a large part of the total heat transfer is occurring in evaporator 1. At $P_2 = 2.6$ bar, the lower bubble point temperatures for the rich and lean streams, have enabled the minimum temperature difference to be reached in both of the following two locations: the bubble point for the rich stream and the outlet of evaporator 1 (state 10 and 15). By increasing the intermediate pressure further, the bubble point temperatures are lowered such that the pinch point is only located at the outlet of evaporator 1 (state 10 and 15). In Fig. 4 (a) there exists an optimum line, separating the regions with pinch point locations at the rich stream bubble point and pinch point locations at the outlet of evaporator 1 (state 10 and 15). When $P_5 = 5.3$ bar, the intermediate pressure is $P_2 = 2.6$ bar at the optimum line, corresponding to the best performing solution with two locations for the minimum pinch point temperature.

For a fixed boiler pressure, the optimization of the intermediate pressure is a matter of maximizing $\dot{m}_{wf}$, which is, considering equation (7), a compromise between reducing the boiler outlet enthalpy ($h_{hf,o}$) and increasing the combined enthalpy of the rich and lean streams at the inlet to the boiler, i.e., the term

$$h_{eff} = h_{13}\left(1 - \frac{Y_{wf} - Y_r}{Y_l - Y_r}\right) + h_9\frac{Y_{wf} - Y_r}{Y_l - Y_r} \tag{10}$$

Since the hot fluid mass flow is multiplied with the numerator in equation (7), the influence of $h_{hf,o}$ is much larger than h_{eff} in determining the optimum intermediate pressure. From Fig. 4 (b) one sees that the optimum intermediate pressure ($P_2 = 2.6$ bar) is also the case with the lowest hot fluid outlet temperature.

Figure 5 shows $\dot{Q}T$-diagrams of the recuperator for (a) $P_2 = 2.2$ bar, (b) $P_2 = 2.6$ bar and (c) $P_2 = 3.2$ bar. For all three cases, the hot stream exits in a two-phase state. As the intermediate pressure increases, the bubble point for the cold stream moves to the right in the $\dot{Q}T$-diagram, while the dew point point for the hot stream moves to the left. At $P_2 \simeq 3.0$ bar

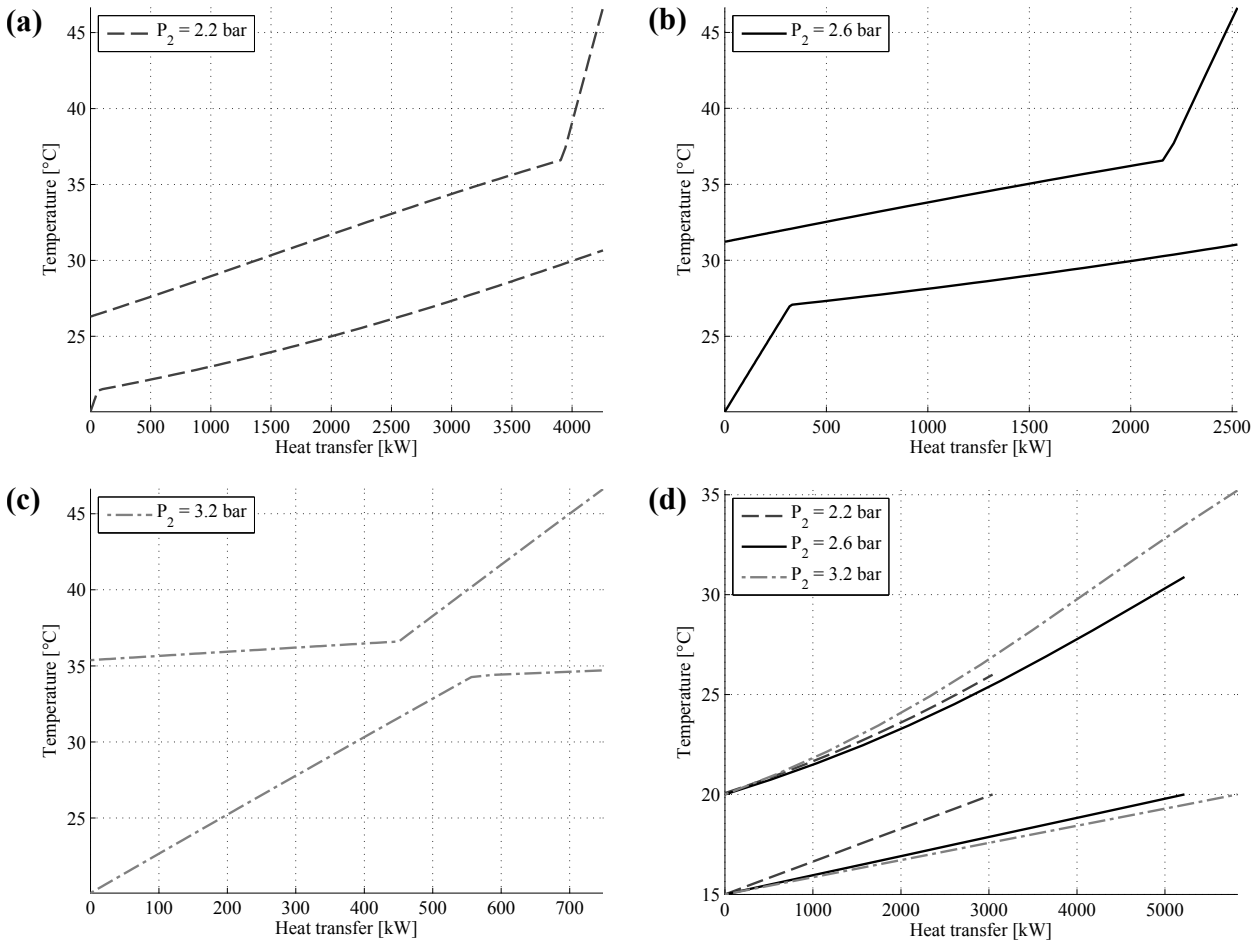

Figure 5: $\dot{Q}T$-diagram of the recuperator for (a) $P_2 = 2.2$ bar, (b) $P_2 = 2.6$ bar, (c) $P_2 = 3.2$ bar, and (d) $\dot{Q}T$-diagrams of the condenser for the three different intermediate pressures with $P_5 = 5.3$ bar

these two points pass each other. When this happens, the intermediate pressure can be increased with no effect on the outlet state of the hot stream in the recuperator, thereby fixing the amount of heat transferred. A further increase of the intermediate pressure does therefore only have a limited effect on the mass flow and composition of the separated lean and rich streams. The crossing of the bubble point and the dew point is observed in Fig. 4 (a) as the flattening of the surface at $P_2 \geq 3$ bar. For low intermediate pressures, this analysis indicates that it is beneficial to transfer less heat in the recuperator. This suggests that the recuperator pinch point ΔT_{recu} should be an optimization parameter rather than a fixed given value, since the lowest possible pinch point does not necessarily result in optimum cycle conditions.

Figure 5 (d) shows a $\dot{Q}T$-diagram of the condenser, illustrating how the condensation process is affected by the intermediate pressure. The condensation pressure is in this case not

affected by changes in the intermediate pressure; however, for fluids with a lower temperature glide or a larger curvature of the condensation temperature profile, it is possible that a low intermediate pressure necessitates a higher condensation pressure. For the $P_2 = 2.6$ bar and $P_2 = 3.2$ bar cases, it is possible to reduce the cooling water mass flow, thereby allowing the cooling water outlet temperature to increase without violating the condenser pinch point. This results in a lower power consumption of the cooling water pump, with a positive effect on the performance of the system.

4.1.2. Evaporator 1 outlet temperature

Figure 6 (a) shows a plot of the net power as a function of the temperature at the outlet of evaporator 1 (T_{10}) and the intermediate pressure (P_2), with indication of the location of the pinch point in the boiler for all plotted solutions and a line representing the case where $x_{10} = 0$. This plot is produced for the isobutane/pentane (0.62/0.38) mixture with $x_5 = 1$. The maximum net power is found when the temperature profile allows two minimum pinch point locations, in either of the following two combinations: the pinch points are at the bubble point for the rich stream and at the bubble point for the lean stream, or at the bubble point for the rich stream and at the inlet to evaporator 2 (state 4).

When P_2 is fixed, T_{10} does not affect the boiler inlet or outlet conditions on the working fluid side, but only the pinch point location, since the working fluid condition at the boiler outlet (state 5) is fixed, and the conditions of the lean and the rich streams are determined by P_2 independently of T_{10}. Figure 6 (b) shows a $\dot{Q}T$-diagram of boiling for $P_2 = 2.6$ bar, where the heat transfer process is illustrated for two cases with $T_{10} = 50$ °C and $T_{10} = 60$ °C. As previously mentioned, it is not possible to define both $x_{10} = 0$ and $x_{15} = 1$ for the OSC, due to the simplified creation of the lean and rich streams. The streams are therefore not in equilibrium prior to mixing. This results in a temperature change after mixing, which is observed as a discontinuity in the $\dot{Q}T$-diagram. When $T_{10} = 50$ °C, the temperature increases after mixing, thus necessitating an increase in the hot fluid outlet temperature, in order to avoid a pinch point violation, with a resulting negative impact on performance. When $T_{10} = 60$ °C, the temperature decreases after mixing, and the performance is therefore not affected negatively by the temperature change of the mixing process. This suggests that the non-equilibrium conditions prior to mixing do not affect performance negatively if T_{10} is chosen above a certain value. For the present case, $T_{10} \geq 55$ °C ensures no performance reduction due to this effect; see Fig. 6 (a) for $P_2 = 2.6$ bar.

The parameter studies suggest that the intermediate pressure and the temperature after evaporator 1 (T_{10}) must be selected in combination in order to reach maximum performance.

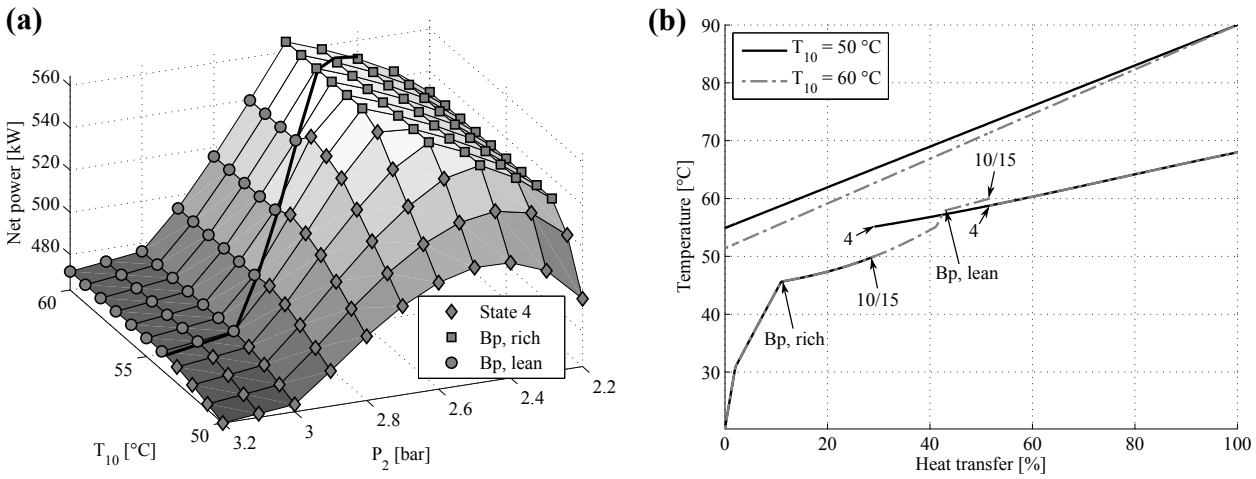

Figure 6: (a) the net power as a function of T_{10} and P_2 for fixed $P_5 = 5.3$ bar and $x_5 = 1$, with indication of the location of the pinch point in the boiler for all plotted solutions and a line representing the case where $x_{10} = 0$, and (b) a $\dot{Q}T$-diagram of boiling with $P_2 = 2.6$ bar and $P_5 = 5.3$ bar

When the two parameters are optimally selected, the temperature profile in the boiler is adjusted such that the minimum pinch point temperature difference is reached at two locations. The results in Fig. 6 (a) indicate that the intermediate pressure is the most important of the two parameters, since the net power is independent of T_{10} at high values of T_{10}.

4.2. Heat transfer analysis of evaporator 1

In this section the results from a preliminary heat transfer analysis of evaporator 1 are presented, for the isobutane/pentane (0.62/0.38) mixture with $x_{10} = 0$, $x_5 = 1$, $P_5 = 5.3$ bar and $P_2 = 2.6$ bar. Figure 7 illustrates the design requirements of evaporator 1 which result from assuming the temperatures of the lean and the rich stream to be equal throughout the heat exchanger. The y-axis shows the local $\bar{U}A$ divided by $\bar{U}A_{tot}/n_{evap}$, which is the total $\bar{U}A$-value of evaporator 1 ($\bar{U}A_{tot}$) divided by the number of control volumes (n_{evap}), representing the average $\bar{U}A$ value per control volume. $\bar{U}A/(\bar{U}A_{tot}/n_{evap})$ is selected as the plotted function in order to ensure that the y-axis is independent of the number of control volumes chosen.

Initially, the lean stream requires a larger $\bar{U}A$-value than the rich stream, because the mass flow of the lean stream is larger. The $\bar{U}A$ requirement increases steadily for both streams, since the temperature profiles of the working fluid and the hot fluid approach each other, thus reducing the temperature difference. In this part of the heat exchanger, the ratio of the $\bar{U}A$ requirement for the two streams is almost constant for each control volume. At $T = 45.6$ °C an extreme increase in the $\bar{U}A$ requirement for the rich stream is observed.

This is the temperature at which the bubble point for the rich stream is reached. When evaporation starts, the temperature increase per input of heat is dramatically reduced, and in order to maintain the equal temperature increase of the two streams, it is necessary to increase the heat input to the rich stream by increasing the $\bar{U}A$-value assigned to the rich stream side. For the lean side, a small reduction in the $\bar{U}A$ requirement is observed when the bubble point for the rich stream is reached. This is due to the change in the temperature profile at the bubble point (see Figure 4 (b)), which increases the temperature difference and thus reduces the required $\bar{U}A$-value. The evaporation of the rich stream is completed at $T = 55.1$ °C. After this point, the $\bar{U}A$-value requirement of the rich stream is again lower than that of the lean stream continuing the trend from the preheating stage. At the outlet of evaporator 1, the lean stream has reached the bubble point and the rich stream is slightly superheated.

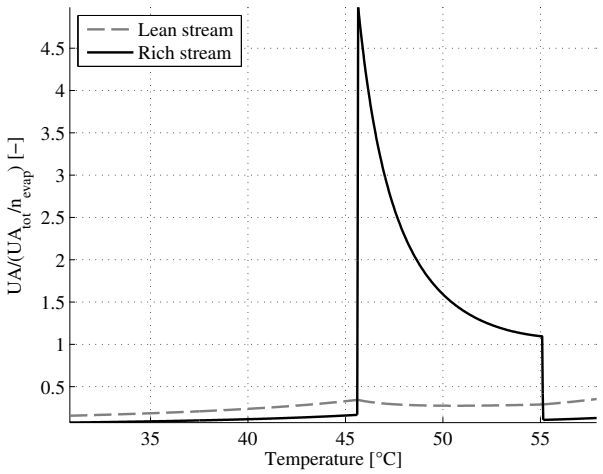

Figure 7: An illustration of the $\bar{U}A$ requirement in evaporator 1 for the lean and the rich stream

This analysis highlights the practical challenges which arise from the assumption of equal temperature rise during heating of the rich and lean streams. The difficulties occur due to the sudden change in heat requirement of the rich stream when it starts to evaporate. In order to accommodate this, a larger heat transfer area must be assigned to the rich stream, suggesting a geometry change in the heat exchanger at this location. At part load conditions, it is not guaranteed that evaporation of the rich stream initiates at the same location, and even at full load, fouling may change the location of the rich stream bubble point over time. In practise it will therefore be necessary to accept some deviation from the equal temperature heating assumption. This does negatively impact the performance of the OSC; however, taking into account the high potential illustrated for the isobutane/pentane

mixture at $T_{hf,i} = 90$ °C, it is reasonable to expect a performance benefit for the OSC, even at uneven heating conditions.

A practical design approach could be to divide the heat exchanger into three parts corresponding to the three zones, defined for the rich stream as: preheating, evaporation and superheating. In each of the three parts, a fixed heat transfer area is designated for the rich and the lean stream. To reduce the complexity of the design of evaporator 1, the last zone can be removed by defining a constraint of $x_{15} = 1$ for the rich stream instead of $x_{10} = 0$ for the lean stream. This removes the superheat zone from the heat exchanger and reduces the number of zones to two.

4.3. Comparison to the ORC

With the OSC it is possible to optimize the boiling process while maintaining a low pressure in the boiler. This is opposed to the transcritical ORC where a performance increase is obtained at the expense of a high boiler pressure compared to the subcritical ORC. In Fig. 8 the optimized OSCs from Tables 3 and 4 are compared based on boiler pressure and net power output with optimized subcritical and transcritical ORCs (both mixtures and pure fluids) from ref. [18]. In ref. [18], the same assumptions for the hot fluid, the ambient conditions and component performance parameters (heat exchanger pinch points and pump and turbine efficiencies) as in the present study have been used. It should be noted that the ORC layout used in ref. [18] does not include a recuperator. However, when we compare the net power outputs of the ORCs with recupertors to ORCs without recuperators the relative differences are below 0.1 % for the working fluids and hot fluid cases investigated in this paper. The small differences are due to changes in the pinch point locations in the condensers. Moreover, previous studies from the scientific literature have evaluated the benefits of the recuperator, and found that the recuperator did not increase the net power output in cases where there is no limit on the hot fluid outlet temperature [26–28]. It is therefore reasonable to compare the net power outputs of OSCs to those of simple ORCs without recuperators.

The two plots in Fig. 8 illustrate that the transcritical ORCs in general give higher net power outputs than the subcritical ORCs, and that the boiler pressures needed for the transcritical cycles are significantly larger than for the subcritical cycles. Figure 8 (a) shows the comparison for $T_{hf,i} = 120$ °C, where the OSCs are located in the same region as the subcritical ORCs. In the figure, the lines connect ORCs and OSCs using the same working fluids. The same comparison for $T_{hf,i} = 90$ °C is illustrated in Fig. 8 (b). Here the OSCs attain higher net power outputs than the subcritical ORCs at low boiler pressures. The OSC

does thereby give access to a new domain in the pressure-power diagram, enabling high net power outputs at low boiler pressures. For both hot fluid inlet temperatures the optimum pressure for the ORCs and OSCs using the same working fluids obtain similar values.

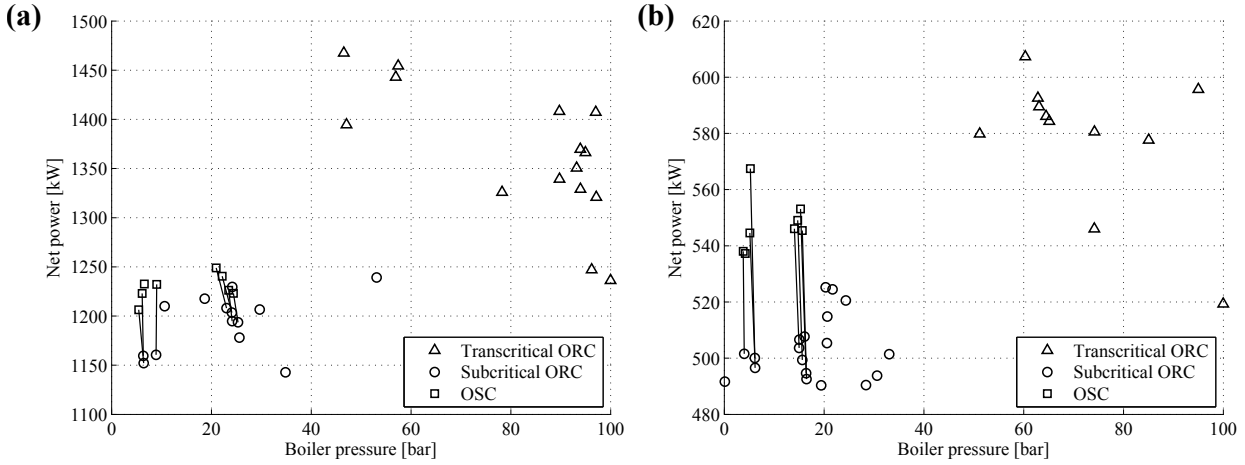

Figure 8: Comparison of OSCs and simple ORCs based on net power and boiler pressure for (a) $T_{hf,i}$ = 120 °C and (b) $T_{hf,i}$ = 90 °C with lines connecting ORCs and OSCs using the same working fluids

Table 5: Comparison of the OSC and the simple ORC based on net power and pressure levels for $T_{hf,i}$ = 120 °C

Working fluids	Cycle	P_{boil} [bar]	P_{cond} [bar]	$\dot{W}_{NET}$ [kW]	$\frac{\dot{W}_{ORC}-\dot{W}_{OSC}}{\dot{W}_{OSC}}$ [%]
propane/isobutane	OSC	21.0	6.6	1249	-
R218	ORC	46.5	8.5	1467	17.4
R1234yf	ORC	24.2	6.8	1230	-1.5

Tables 5 and 6 show a comparison of OSCs and simple ORCs for hot fluid inlet temperatures of 120 °C and 90 °C, respectively. The fluids chosen for this comparison are the OSCs with highest net power outputs (propane/isobutane and isobutane/pentane), the ORCs with the highest net power outputs (R218 and ethane/propane) and the best performing ORCs with pressure levels similar to those of the optimal OSCs (R1234yf and butane/isopentane). For both hot fluid inlet temperatures, the ORCs obtain the highest performance when high pressures are allowed, while the OSCs reach the highest net power when the the cycles are compared at low pressures. The low temperature case represent the most promising application for the OSC, since the performance of an ORC (butane/isopentane) with similar cycle pressures obtain 11.5 % lower net power. High pressures are undesirable since they are

Table 6: Comparison of the OSC and the simple ORC based on net power and pressure levels for $T_{hf,i} = 90$ °C

Working fluids	Cycle	P_{boil} [bar]	P_{cond} [bar]	$\dot{W}_{NET}$ [kW]	$\frac{\dot{W}_{ORC}-\dot{W}_{OSC}}{\dot{W}_{OSC}}$ [%]
isobutane/pentane	OSC	5.2	2.1	567	-
ethane/propane	ORC	60.3	32.3	607	7.1
butane/isopentane	ORC	4.0	1.6	502	-11.5

related to high safety hazards and costs [29, 30]. The OSC technology thereby represents an alternative thermodynamic cycle, which enables a performance increase compared to the subcritical ORC, without introducing the challenges related to high pressures; however, the OSC introduces additional complexity compared to the ORC.

Compared to the ORC, the OSC includes additional heat exchangers, but the amount of additional heat transfer area needed for the OSC process depends on the amount of transferred heat, the temperature difference available and the overall heat transfer coefficient for the heat exchangers. In the following, the $\bar{U}A$-values of the OSCs and the ORCs are compared, meaning that differences in overall heat transfer coefficients are disregarded. Tables 7 and 8 list the $\bar{U}A$-values for the heat exchangers in the OSCs and the recuperated ORCs, and a comparison of the relative difference between the total $\bar{U}A$-values of the two cycles for $T_{hf,i} = 120$ °C and $T_{hf,i} = 90$ °C, respectively.

Table 7: Comparison of $\bar{U}A$-values for the OSC and the ORC processes for $T_{hf,i} = 120$ °C

$\bar{U}A$ [kW/K]	ibut/ipen	but/ipen	ibut/pen	but/pen	pro/ibut	pro/but	pro/ipen	pro/pen
OSC								
Condenser 1	1649	1909	1040	1436	1934	1911	1530	1756
Recuperator	170	121	484	154	135	124	281	211
Condenser 2	189	161	421	245	169	151	173	103
Preheater	10	8	33	14	10	9	13	8
Evaporator 1	342	246	385	284	292	287	517	598
Evaporator 2	296	357	392	364	329	341	159	47
Superheater	0	7	0	25	30	24	1	0
Total	2656	2810	2755	2521	2900	2848	2675	2724
ORC								
Condenser	2042	2064	2021	2017	2272	2192	2087	2053
Preheater	175	153	176	153	239	246	247	244
Evaporator	365	370	361	369	351	342	341	340
Superheater	0	0	0	0	1	3	4	6
Total	2583	2588	2558	2538	2863	2783	2679	2643
Comparison								
$\Delta\bar{U}A_{tot}$ [%]	2.8	8.6	7.7	-0.7	1.3	2.3	-0.2	3.1

The $\bar{U}A$-values for condenser 1 of the OSCs are in general lower than those for the ORC condensers. This is because the temperature glides of condensation at optimum conditions

Table 8: Comparison of $\bar{U}A$-values for the OSC and the ORC processes for $T_{hf,i} = 90$ °C

$\bar{U}A$ [kW/K]	ibut/ipen	but/ipen	ibut/pen	but/pen	pro/ibut	pro/but	pro/ipen	pro/pen
OSC								
Condenser 1	968	1249	750	1115	1257	1088	796	836
Recuperator	188	89	403	86	96	140	296	262
Condenser 2	241	169	370	172	172	195	314	258
Preheater	13	7	21	6	8	9	19	16
Evaporator 1	202	156	258	154	165	176	226	384
Evaporator 2	306	291	315	291	277	286	347	184
Superheater	40	38	0	41	57	50	0	0
Total	1958	2000	2117	1866	2032	1944	1998	1941
ORC								
Condenser	1249	1293	1211	1201	1366	1285	1219	1189
Preheater	76	69	75	65	89	88	88	86
Evaporator	310	312	313	318	306	308	308	309
Superheater	0	0	0	0	0	0	0	1
Total	1635	1674	1599	1584	1762	1681	1615	1586
Comparison								
$\Delta\bar{U}A_{tot}$ [%]	19.8	19.5	32.3	17.8	15.4	15.6	23.7	22.4

are larger for the OSCs compared to the ORCs, which results in larger temperature differences of condensation for the OSCs. The larger temperature glides for the OSCs also allow more heat to be transferred in the recuperator, and the OSC recuperators therefore require larger $\bar{U}A$-values than the ORC recuperators. On the other hand, the $\bar{U}A$-values required for the boilers of the OSCs (preheater, evaporator 1, evaporator 2 and superheater) are generally higher than those of the ORC boilers (preheater, evaporator and superheater). The need for condensing the separated vapour in condenser 2 is an additional contribution, which increases the required $\bar{U}A$-value for the OSCs compared to the ORCs.

For $T_{hf,i} = 120$ °C, the difference in $\bar{U}A$-values for the OSC and the ORC processes are 7.0 % and 6.5 % for butane/isopentane and isobutane/pentane, respectively, while minor differences are observed for the remaining fluids. For $T_{hf,i} = 90$ °C, the $\bar{U}A$-values are 14.1 to 30.6 % higher for the OSCs. The higher relative increases at this hot fluid inlet temperature are due to lower benefits of the high temperature glide of condensation for condenser 1, and due to larger $\bar{U}A$-values for condenser 2 (except for isobutane/pentane and butane/pentane) compared to the $T_{hf,i} = 120$ °C case. The lower absolute values of total $\bar{U}A$ at $T_{hf,i} = 90$ °C also contribute to the larger relative differences.

The comparison based on $\bar{U}A$-values at $T_{hf,i} = 120$ °C indicates that the OSC and the ORC require the same total $\bar{U}A$-value, suggesting similar costs for the heat exchangers. For the $T_{hf,i} = 90$ °C case, the $\bar{U}A$-values required for the OSCs are larger than those of the ORCs, indicating higher costs for the heat exchangers in the OSC.

Whether or not the performance benefits of the OSC process justify the additional com-

plexity compared to the ORC from an economic standpoint is a subject for further analysis; however, the present thermodynamic analysis indicates that the split evaporation represents a possible cycle improvement even in its simplest implementation.

4.4. Comparison to the Kalina split-cycle

The primary difference between the OSC and the Kalina split-cycle is the creation of the split streams. In the OSC the compositions of the rich and lean streams are not changed from the outlet of the separator to the inlet to the boiler. In the Kalina split-cycle configuration investigated by Larsen et al. [16] and Nguyen et al. [17], the rich stream is split once (creating two streams) and the lean stream is split twice (creating three streams). After these splits, the two rich streams and two of the lean streams are mixed in pairs, and the remaining lean stream is returned to the condenser. This makes it possible to define the outlet conditions for evaporator 1 as saturated vapour for the rich stream and saturated liquid for the lean stream, referred to by Larsen et al. [16] as the boiler constraint. The boiler constraint ensures that no temperature change occurs when the streams are mixed after evaporator 1, since the outlet streams are in thermodynamic equilibrium. In the OSC, the outlet streams from evaporator 1 are not in thermodynamic equilibrium, resulting in a temperature change after mixing, which could possibly entail an undesirable temperature profile. The parameter study for the outlet temperature of evaporator 1 suggested that, if the heating load is divided between evaporator 1 and 2 in a desirable way, a pinch point violation, caused by a temperature increase after mixing, can be avoided.

The additional freedom in the design of the rich and lean stream compositions makes it reasonable to expect that the Kalina split-cycle can obtain higher performance compared to the OSC, due to both the possibility of optimizing the rich and the lean stream compositions and the possibility of having different compositions through the expander and condenser 1. However, the OSC is an attractive technology, since it includes the thermodynamically beneficial split evaporation, with a cycle layout which is much simpler than the Kalina split-cycle. The simpler configuration is beneficial in terms of lower investment costs, controllability and lower pressure losses owing to the fewer components.

5. Conclusion

This paper presents a first study on the novel OSC. Optimizations of the OSC for eight different hydrocarbon mixtures for hot fluid temperatures at 120 °C and 90 °C indicate that the largest performance increase compared to the ORC is obtained when the hot fluid

inlet temperature is low. The most promising of the eight mixtures for the 90 °C hot fluid inlet temperature case is an isobutane/pentane mixture, which reaches a 14.5 % higher net power output than an optimized ORC using the same mixture. This performance increase is obtained due to an improvement of the boiling process.

Two parameter studies, of the intermediate pressure and the outlet temperature of evaporator 1, carried out for the promising isobutane/pentane mixture, indicate that optimum conditions are found when the temperature profile enables two locations of minimum pinch point temperature differences.

The improvement in the boiling process of the OSC compared to the ORC is achieved at the cost of increased cycle complexity. Additionally, the results suggest larger heat transfer areas for the OSC when the hot fluid inlet temperature is 90 °C. Compared to the Kalina split-cycle, the OSC is a less complex power cycle. The OSC concept does thereby represent a compromise between the complex Kalina split-cycle and the simpler ORC, and thus may serve as a viable power cycle for low grade heat utilization.

Acknowledgements

Part of the work presented in this paper has been conducted within the frame of the THERMCYC project ("Advanced thermodynamic cycles utilising low-temperature heat sources"; see http://www.thermcyc.mek.dtu.dk/) funded by InnovationsFonden, The Danish Council for Strategic Research in Sustainable Energy and Environment. The financial support is gratefully acknowledged. Susan Canali is acknowledged for her proof reading assistance.

References

[1] S. Quoilin, M. van den Broek, S. Declaye, P. Dewallef, V. Lemort, Techno-economic survey of Organic Rankine Cycle (ORC) systems, Renew. Sustain. Energy Rev. 22 (2013) 168–186. doi:10.1016/j.rser.2013.01.028.

[2] H. Chen, D. Y. Goswami, E. K. Stefanakos, A review of thermodynamic cycles and working fluids for the conversion of low-grade heat, Renew. Sustain. Energy Rev. 14 (9) (2010) 3059–3067. doi:10.1016/j.rser.2010.07.006.

[3] Y.-J. Baik, M. Kim, K.-C. Chang, Y.-S. Lee, H.-K. Yoon, A comparative study of power optimization in low-temperature geothermal heat source driven R125 transcritical cycle and HFC organic Rankine cycles, Renew. Energy 54 (2013) 78–84. doi:10.1016/j.renene.2012.08.055.

[4] G. Angelino, P. Colonna, Multicomponent working fluids for organic Rankine cycles (ORCs), Energy 23 (6) (1998) 449–463. doi:dx.doi.org/10.1016/S0360-5442(98)00009-7.

[5] F. Heberle, M. Preißinger, D. Brüggemann, Zeotropic mixtures as working fluids in Organic Rankine Cycles for low-enthalpy geothermal resources, Renew. Energy 37 (1) (2012) 364–370. doi:10.1016/j.renene.2011.06.044.

[6] S. Lecompte, B. Ameel, D. Ziviani, M. van den Broek, M. De Paepe, Exergy analysis of zeotropic mixtures as working fluids in Organic Rankine Cycles, Energy Convers. Manag. 85 (2014) 727–739. doi:10.1016/j.enconman.2014.02.028.

[7] T. Weith, F. Heberle, M. Preißinger, D. Brüggemann, Performance of Siloxane Mixtures in a High-Temperature Organic Rankine Cycle Considering the Heat Transfer Characteristics during Evaporation, Energies 7 (9) (2014) 5548–5565. doi:10.3390/en7095548.

[8] M. Chys, M. van den Broek, B. Vanslambrouck, M. De Paepe, Potential of zeotropic mixtures as working fluids in organic Rankine cycles, Energy 44 (1) (2012) 623–632. doi:10.1016/j.energy.2012.05.030.

[9] X. Zhang, M. He, Y. Zhang, A review of research on the Kalina cycle, Renew. Sustain. Energy Rev. 16 (7) (2012) 5309–5318. doi:10.1016/j.rser.2012.05.040.

[10] H. D. M. Hettiarachchi, M. Golubovic, W. M. Worek, Y. Ikegami, The Performance of the Kalina Cycle System 11(KCS-11) With Low-Temperature Heat Sources, J. Energy Resour. Technol. 129 (3) (2007) 243. doi:10.1115/1.2748815.

[11] P. Bombarda, C. M. Invernizzi, C. Pietra, Heat recovery from Diesel engines: A thermodynamic comparison between Kalina and ORC cycles, Appl. Therm. Eng. 30 (2-3) (2010) 212–219. doi:10.1016/j.applthermaleng.2009.08.006.

[12] A. Modi, F. Haglind, Performance analysis of a Kalina cycle for a central receiver solar thermal power plant with direct steam generation, Appl. Therm. Eng. 65 (1-2) (2014) 201–208. doi:10.1016/j.applthermaleng.2014.01.010.

[13] A. Modi, F. Haglind, Thermodynamic optimisation and analysis of four Kalina cycle layouts for high temperature applications, Appl. Therm. Eng. 76 (2015) 196–205. doi:10.1016/j.applthermaleng.2014.11.047.

[14] J. Bao, L. Zhao, Exergy analysis and parameter study on a novel auto-cascade Rankine cycle, Energy 48 (1) (2012) 539–547. doi:10.1016/j.energy.2012.10.015.

[15] A. I. Kalina, Method of generating energy, Patent, US 4548043 (1985).

[16] U. Larsen, T.-V. Nguyen, T. Knudsen, F. Haglind, System analysis and optimisation of a Kalina split-cycle for waste heat recovery on large marine diesel engines, Energy 64 (2014) 484–494. doi:10.1016/j.energy.2013.10.069.

[17] T.-V. Nguyen, T. Knudsen, U. Larsen, F. Haglind, Thermodynamic evaluation of the Kalina split-cycle concepts for waste heat recovery applications, Energy 71 (2014) 277–288. doi:10.1016/j.energy.2014.04.060.

[18] J. G. Andreasen, U. Larsen, T. Knudsen, L. Pierobon, F. Haglind, Selection and optimization of pure and mixed working fluids for low grade heat utilization using organic Rankine cycles, Energy 73 (2014) 204–213. doi:10.1016/j.energy.2014.06.012.

[19] Mathworks, Matlab 2012b documentation., Tech. rep., Massachusetts, The United States of America (2012).

[20] E. W. Lemmon, M. Huber, M. McLinden, NIST Standard Reference Database 23: Reference Fluid Thermodynamic and Transport Properties-REFPROP, Version 9.0, National Institute of Standards

and Technology, Standard Reference Data Program, Gaithersburg, 2010, www.nist.gov.

[21] E. W. Lemmon, M. O. McLinden, W. Wagner, Thermodynamic properties of propane. III. A reference equation of state for temperatures from the melting line to 650 K and pressures up to 1000 MPa, J. Chem. Eng. Data 54 (12) (2009) 3141–3180. doi:10.1021/je900217v.

[22] D. Bücker, W. Wagner, Reference equations of state for the thermodynamic properties of fluid phase n-butane and isobutane, J. Phys. Chem. Ref. Data 35 (2) (2006) 929–1019. doi:10.1063/1.1901687.

[23] R. Span, W. Wagner, Equations of State for Technical Applications. II. Results for Nonpolar Fluids, Int. J. Thermophys. 24 (1) (2003) 41–109. doi:10.1023/A:1022310214958.

[24] E. W. Lemmon, R. Span, Short fundamental equations of state for 20 industrial fluids, Vol. 51, 2006. doi:10.1021/je050186n.

[25] O. Kunz, W. Wagner, The GERG-2008 wide-range equation of state for natural gases and other mixtures: An expansion of GERG-2004, J. Chem. Eng. Data 57 (11) (2012) 3032–3091. doi:10.1021/je300655b.

[26] D. Maraver, J. Royo, V. Lemort, S. Quoilin, Systematic optimization of subcritical and transcritical organic Rankine cycles (ORCs) constrained by technical parameters in multiple applications, Appl. Energy 117 (2014) 11–29. doi:10.1016/j.apenergy.2013.11.076.

[27] W. Li, X. Feng, L. Yu, J. Xu, Effects of evaporating temperature and internal heat exchanger on organic Rankine cycle, Appl. Therm. Eng. 31 (17-18) (2011) 4014–4023. doi:10.1016/j.applthermaleng.2011.08.003.

[28] Y. Dai, J. Wang, L. Gao, Parametric optimization and comparative study of organic Rankine cycle (ORC) for low grade waste heat recovery, Energy Convers. Manag. 50 (3) (2009) 576–582. doi:10.1016/j.enconman.2008.10.018.

[29] C. R. Kuo, S. W. Hsu, K. H. Chang, C. C. Wang, Analysis of a 50kW organic Rankine cycle system, Energy 36 (10) (2011) 5877–5885. doi:10.1016/j.energy.2011.08.035.

[30] U. Drescher, D. Brüggemann, Fluid selection for the Organic Rankine Cycle (ORC) in biomass power and heat plants, Appl. Therm. Eng. 27 (2007) 223–228. doi:10.1016/j.applthermaleng.2006.04.024.